Chemical Science

ROYAL SOCIETY OF CHEMISTRY

EDGE ARTICLE

View Article Online
View Journal | View Issue

Cite this: *Chem. Sci.*, 2025, **16**, 10983

All publication charges for this article have been paid for by the Royal Society of Chemistry

"Three functions in one": multifunctional rare-earth cyamelurates with magnetism, luminescence, and giant optical nonlinearity†

Jing Zhang, [a] Yuxiao Liu,[b] Fangyan Wang, [b] Pifu Gong, [c] Zhaoyi Li,[d] Xinyuan Zhang, *[a] Fei Liang, *[b] Shu Guo, [d] Zhanggui Hu[a] and Yicheng Wu[ab]

Received 17th February 2025
Accepted 6th May 2025

DOI: 10.1039/d5sc01230a

rsc.li/chemical-science

A highly-integrated optical device requires multifunctional crystals, which respond strongly to external stimuli, such as photoluminescence, nonlinear polarization, and magnetoelectric coupling. However, it is usually difficult for these functions to coexist in a single-phase crystal, and can even be incompatible. Here, we propose a 'unit assembly' strategy in rare-earth cyamelurates, which combines active rare-earth ions (Gd^{3+}, Y^{3+}, Lu^{3+}) and π-conjugated $[H_xC_6N_7O_3]^{(3-x)-}$ units into one crystal with an aligned arrangement. For the first time, we synthesized three new rare-earth cyamelurate crystals $RE(H_{1.5}C_6N_7O_3)_2{\cdot}10H_2O$ (RE = Y, Gd, Lu) by a facile solution method. Benefitting from the strong polarizability and delocalized electrons of the π-conjugated units, all three crystals display giant second-order optical nonlinearity (12–15.3 × KDP), broadband photoluminescence (300–500 nm), and strong anisotropic birefringence (Δn > 0.22) at 1064 nm. Moreover, the Gd-analogue exhibits paramagnetic behaviour in a wide temperature range. These results highlight rare-earth cyamelurates as promising multifunctional optical crystals with three concurrent functional responses, indicating potential applications in next-generation photonics and optoelectronics.

Introduction

The integration of multiple functionalities into a single crystal remains a long-standing challenge in the field of inorganic functional materials. Currently, the composition and structure of functional units are key factors affecting the overall performance of functional materials. Rational design of these building units can effectively improve the optical response of the materials under an external field.[1] In the past thirty years, many nonlinear optical (NLO) crystals with excellent performances have been discovered,[2–9] and several anionic groups have been identified as effective fundamental building blocks for enhancing nonlinear responses.[10–16] These include $(SeO_3)^{2-}$ and $(IO_3)^-$, which possess stereochemically active lone pairs; $(NbO_6)^{7-}$ and $(VO_6)^{7-}$, which exhibit Jahn–Teller effects; and $(BO_3)^{3-}$, $(CO_3)^{2-}$, and $(B_3O_6)^{3-}$, which feature planar π-conjugated groups. Among these various kinds of anions, π-conjugated groups with large optical anisotropy and microscopic second-order susceptibility are regarded as some of the most successful. This has led to the discovery of a series of benchmark crystals, *e.g.* $KBe_2BO_3F_2$ (KBBF), β-BaB_2O_4 (BBO), LiB_3O_5 (LBO), *etc.*[17–19] However, these small π-conjugated units typically exhibit an ultrawide bandgap, thus hindering their fluorescent emission and magnetic responses. Therefore, it remains a great challenge to design multifunctional crystals within an inorganic π-conjugated system.

Recently, metal cyanurates with large π-conjugated $(C_3N_3O_3)^{3-}$ unit have been developed as effective nonlinear optical materials,[20–23] including $KLi(HC_3N_3O_3){\cdot}2H_2O$, $Cs_3Na(H_2C_3N_3O_3)_4{\cdot}3H_2O$, and $RE_5(C_3N_3O_3)(OH)_{12}$ (RE = Y, Yb, and Lu). More interestingly, owing to the reduced forbidden gap of the $(C_3N_3O_3)^{3-}$ unit, several cyanurates display a strong photoluminescence response, such as $Pb(H_2C_3N_3O_3)F$ with blue emission around 482 nm.[24] Besides, $C_4N_3H_6SO_3NH_2$ with a π-conjugated $[C_4N_3H_6]$ group also shows blue-violet and green fluorescence near 360 and 520 nm,[25] thus indicating that the introduction of a large π-conjugated unit could be a feasible strategy to design multifunctional crystals with concurrent optical nonlinearity and photoluminescence.

[a]*State Key Laboratory of Crystal Materials, Tianjin Key Laboratory of Functional Crystal Materials, Institute of Functional Crystals, Tianjin University of Technology, Tianjin 300384, China. E-mail: xyzhang@email.tjut.edu.cn*

[b]*State Key Laboratory of Crystal Materials and Institute of Crystal Materials, Shandong University, Jinan 250100, China. E-mail: liangfei@sdu.edu.cn*

[c]*Functional Crystals Lab, Technical Institute of Physics and Chemistry, Chinese Academy of Sciences, Beijing 100190, China*

[d]*Shenzhen Institute for Quantum Science and Engineering, Southern University of Science and Technology, Shenzhen 518055, China*

† Electronic supplementary information (ESI) available: Experimental section, crystallographic data, PXRD patterns, thermal analysis, IR spectrum, UV–visible–NIR diffuse reflectance spectrum, and band structures. CCDC 2385148–2385150. For ESI and crystallographic data in CIF or other electronic format see DOI: https://doi.org/10.1039/d5sc01230a

Following this design principle, we focused on a large π-conjugated group, $(C_6N_7O_3)^{3-}$, as a building unit for multifunctional optical crystals. Compared to previously studied π-conjugated units, such as $(BO_3)^{3-}$ (conjugated electronic configuration π_4^3), $(CO_3)^{2-}$ (π_4^4), $(B_3O_6)^{3-}$ (π_9^9), and $(C_3N_3O_3)^{3-}$ (π_9^9), the $(C_6N_7O_3)^{3-}$ unit possesses the ultra-large π-conjugated electron configuration π_{16}^{17}, indicating its strong p_π–p_π conjugated interaction and delocalized electron distribution on the planar ring. In 2022, we synthesized the first SHG active alkali cyamelurate, $K_3C_6N_7O_3\cdot 2H_2O$, which exhibited excellent nonlinear optical properties (SHG ~4 × KDP, $\Delta n_{cal} > 0.446$).[26] Subsequently, iso-cyamelurates $(H_xC_6N_7O_3)^{x-3}$ ($x = 1, 2$) were also explored as a promising candidate with both enhanced SHG efficiency and birefringence, including $A_{0.5}H_2C_6N_7O_3\cdot 4H_2O$ (A = Ca^{2+}, Sr^{2+}, Ba^{2+}) (SHG > 5 × KDP, E_g ~4.0 eV), $Cd(H_2C_6N_7O_3)_2\cdot 4H_2O$ (SHG ~1.4 × KDP, E_g ~4.0 eV) $Sr[H_2C_6N_7O_3]_2\cdot 4H_2O$, and $Er(C_6N_7O_3)\cdot 5H_2O$.[27–31] However, the integration of strong optical nonlinearity, broadband photoluminescence, and magnetic response has never been realized in the cyamelurate system.

Here, we propose a 'unit assembly' strategy to design multifunctional crystals, which combines the active metal ion and π-conjugated $[H_xC_6N_7O_3]^{(3-x)-}$ unit into rare-earth cyamelurates. The rare-earth ions are considered to enrich the optical response of cyamelurate materials in the following ways: (i) Closed-shell configurations and half-filled 4f orbitals of rare-earth cations (Y^{3+}, La^{3+}, and Lu^{3+}) can inhibit d–d and f–f electronic transitions, expanding the cutoff edge from the visible to the ultraviolet (UV) region and thus broadening the band gap. (ii) Rare-earth cations usually exhibit strong coordination properties, favoring the alignment of ligand anions in non-centrosymmetric arrangements. (iii) Rare-earth ions may impart intriguing magnetic behavior originating from the 4f electronic configuration. In this work, Y^{3+}, Gd^{3+}, and Lu^{3+} are regarded as key elements to fabricate new SHG-active cyamelurate crystals. Fortunately, three new isostructural rare earth cyamelurates $Y(H_{1.5}C_6N_7O_3)_2\cdot 10H_2O$ (**I**), $Gd(H_{1.5}C_6N_7O_3)_2\cdot 10H_2O$ (**II**), and $Lu(H_{1.5}C_6N_7O_3)_2\cdot 10H_2O$ (**III**) were successfully designed and synthesized by a feasible aqueous solution-cooling method, with strong SHG intensities (>12 × KDP), wide fluorescence, sufficient birefringence (Δn ~0.22 at 1064 nm), and paramagnetic behaviour over a wide temperature range in **II**. The structure–property relationships were investigated through theoretical calculations.

Results and discussion

Crystal structure

Colourless plate-like crystals of the three compounds were obtained, and XRD diffraction (Fig. S1†) was used to confirm the purity of the sample powder. The three $RE(H_{1.5}C_6N_7O_3)_2\cdot 10H_2O$ (RE = Y, Gd, Lu) compounds are isostructural, and all the detailed structural information, additional bond lengths, and bond angle information are listed in Tables 1 and S1–S12.† Herein, only compound **II** is illustrated as an example. $Gd(H_{1.5}C_6N_7O_3)_2\cdot 10H_2O$ (**II**) crystallizes in the acentric orthorhombic *Fdd*2 space group (No. 43). As shown in Fig. 1a, the Gd^{3+} cation is coordinated with eight O atoms, of which the Gd–O distances range from 2.34–2.48 Å. Among the eight coordinated O atoms of the Gd–O polyhedron, the two contributed planar iso-cyamelurate $[H_2C_6N_7O_3]^-$ and $[HC_6N_7O_3]^{2-}$ anion groups are at the angle of ~75.74°, and the dihedral angle is slightly different in **I** and **III** with values of 76.02° and 76.25°, respectively. The stacking pattern of the Gd^{3+} cation is shown in Fig. 1b, and the distances between Gd···Gd interactions are measured as 6.15 Å and 6.58 Å, respectively. Fig. 1c displays the packing diagram with coordinated Gd polyhedra, and the vertical distance between the Gd···Gd plane along the *c*-axis is 5.82 Å, while the

Table 1 Crystal data and structure refinements of $RE(H_{1.5}C_6N_7O_3)_2\cdot 10H_2O$ (RE = Y, Gd, Lu)

	$Y(H_{1.5}C_6N_7O_3)_2\cdot 10H_2O$	$Gd(H_{1.5}C_6N_7O_3)_2\cdot 10H_2O$	$Lu(H_{1.5}C_6N_7O_3)_2\cdot 10H_2O$
Formula weight	708.35	776.69	794.41
Crystal system	Orthorhombic	Orthorhombic	Orthorhombic
Space group	*Fdd*2	*Fdd*2	*Fdd*2
a (Å)	67.056(8)	67.4247(9)	66.982(3)
b (Å)	6.1193(7)	6.14740(10)	6.1537(2)
c (Å)	11.4807(13)	11.6319(3)	11.6511(4)
α (deg)	90	90	90
β (deg)	90	90	90
γ (deg)	90	90	90
V/Å^3	4710.9(9)	4821.27(18)	4802.4(3)
Z	8	8	8
ρ_{calc} (g cm^{-3})	1.997	2.140	2.197
μ (mm^{-1})	2.589	2.862	4.222
F (000)	2880	3080	3136
Flack parameter	0.01(2)	0.04(4)	0.02(3)
Goodness-of-fit on F^2	1.093	1.133	1.146
Reflections collected	27 752	33 858	4777
Final *R* indexes [$I \geq 2\sigma(I)$] [a]	$R_1 = 0.0728$, $\omega R_2 = 0.2150$	$R_1 = 0.0566$, $\omega R_2 = 0.1731$	$R_1 = 0.0492$, $\omega R_2 = 0.1496$
Final *R* indexes [all data] [a]	$R_1 = 0.0801$, $\omega R_2 = 0.2251$	$R_1 = 0.0645$, $\omega R_2 = 0.1808$	$R_1 = 0.0532$, $\omega R_2 = 0.1538$
CCDC no.	2385148	2385149	2385150

[a] $R_1 = \sum||F_o| - |F_c||/\sum|F_o|$, $\omega R_2 = [\sum\omega(F_o^2 - F_c^2)^2/\sum\omega(F_o^2)^2]^{1/2}$.

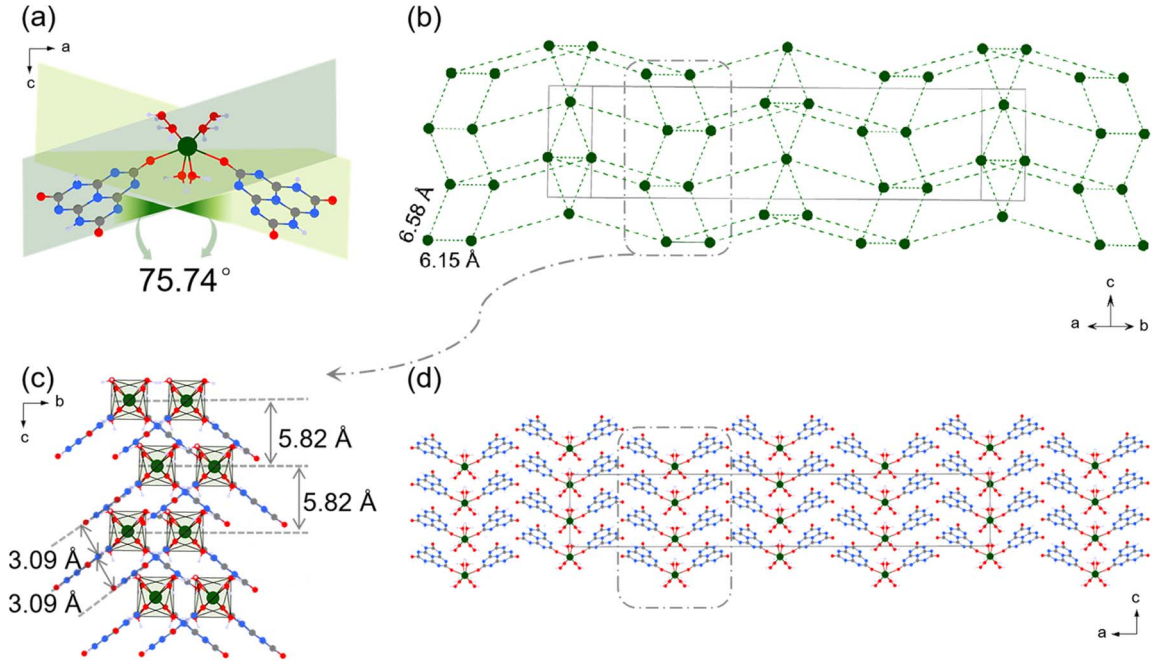

Fig. 1 (a) The coordination environment of Gd^{3+}; (b) the stacking diagram of Gd^{3+} cations; (c) the stacking pattern of Gd^{3+} polyhedra; and (d) the crystal structure of **II**. The olive-green, red, gray, blue, and light gray balls represent Gd, O, C, N, and H, respectively.

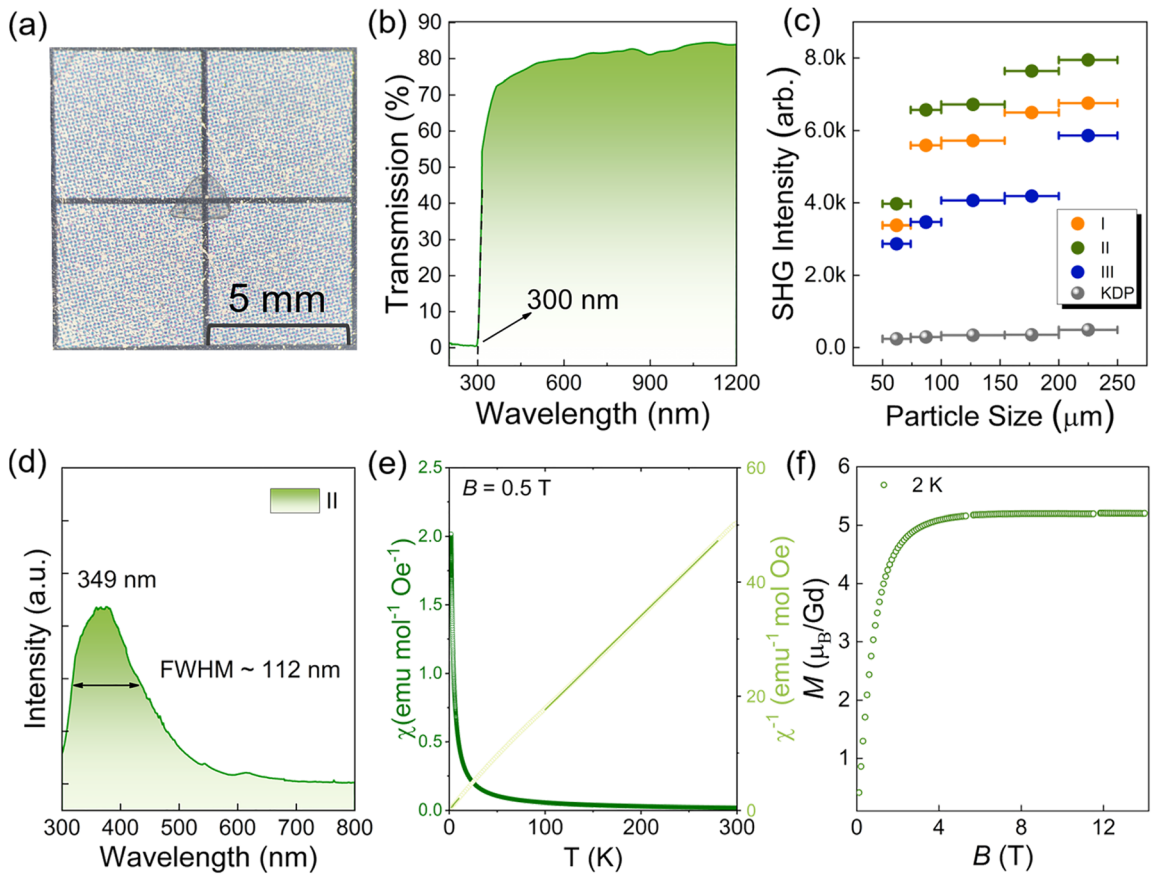

Fig. 2 (a) The grown crystal of **II**. (b) UV-vis-NIR transmittance spectrum of **II**. (c) SHG measurements of the three compounds. (d) Photoluminescent measurements of **II**. (e) χ *versus* temperature of **II** for FC data (green symbol line) and the plot of $1/\chi$ *versus* temperature (light green symbol line). (f) Magnetic susceptibility as a function of the applied field for the **II** samples with Gd.

nearest anion layers are at a distance of 3.09 Å. Interestingly, as the ligand anions are connected on the two sides of the Gd^{3+} cations like the wings of a butterfly, the crystal structure is like an orderly arrangement of butterfly teams (Fig. 1d).

Chemical phase and thermal stability

Fig. S2† displays the results of thermogravimetry (TG) and differential scanning calorimetry (DSC) analysis of compounds **I**, **II**, and **III**. There are generally two weight loss steps in the process of heating, which correspond to the loss of crystalline water starting from 109 °C and sample decomposition occurring around 230 °C. Besides, the powder XRD diffraction confirmed that the sample can match the calculated diffraction peaks after six months in a dryer, indicating the stability of the three hydrates (Fig. S3†).

Linear and nonlinear optical properties

The IR spectrum (Fig. S4†) indicates the presence of the cyamelurate group, in which the absorption peaks at 1654, 1516, 1406, and 1149 cm^{-1} can be attributed to aromatic C-N heterocycles, while bending the vibrational mode of *s*-triazine units can be assigned to peaks at 809 cm^{-1}.[32] The UV-vis transmission spectrum of compound **II** was measured with a transparent crystal plate (Fig. 2a), and the cutoff edge is estimated as 300 nm, corresponding to the band gap of 4.1 eV (Fig. 2b). The diffuse reflection spectra of the three compounds are nearly the same, also indicating the enhanced band gaps ~ 4.0 eV (Fig. S5†), which are far larger than previously reported alkali cyamelurate of $K_3(C_6N_7O_3)$ and $K_3C_6N_7O_3\cdot 2H_2O$, E_g ~3.0 eV.[33] The SHG response of the three compounds was measured by the Kurtz–Perry method[34] under 1064 nm incident light. Samples of **I**, **II**, and **III** respectively display very strong SHG efficiencies of 13.9, 15.3, and 12 × KDP with phase-matching behavior (Fig. 2c), which is the largest among reported metal cyamelurates, such as $Ba(H_2C_6N_7O_3)_2\cdot 8H_2O$ (12 × KDP) and $A_{0.5}H_2C_6N_7O_3\cdot 4H_2O$ (A = Ca^{2+}, Sr^{2+}) (>5 × KDP). Moreover, all three compounds show a broadband UV photoluminescence around 350 nm under the excitation wavelength of 288 nm (Fig. 2d and S6†). The emission spectra exhibit that the full width at half maximum (FWHM) is > 100 nm for compounds **I** and **II**, which is apparently wider than that previously reported in $A_3(C_6N_7O_3)$ (A = Li, Na, K, Rb, Cs) (FWHM ~50 nm), $K_3C_6N_7O_3\cdot 2H_2O$ (~60 nm), $Ca_{0.5}H_2C_6N_7O_3\cdot 4H_2O$ (~82 nm), and $K_{0.5}In_{0.5}(H_2C_6N_7O_3)_2\cdot 9H_2O$ (~88 nm).[35,36] Such wide photoluminescence could be attributed to the reduced bandgap of the cyamelurate unit and the possible electron-

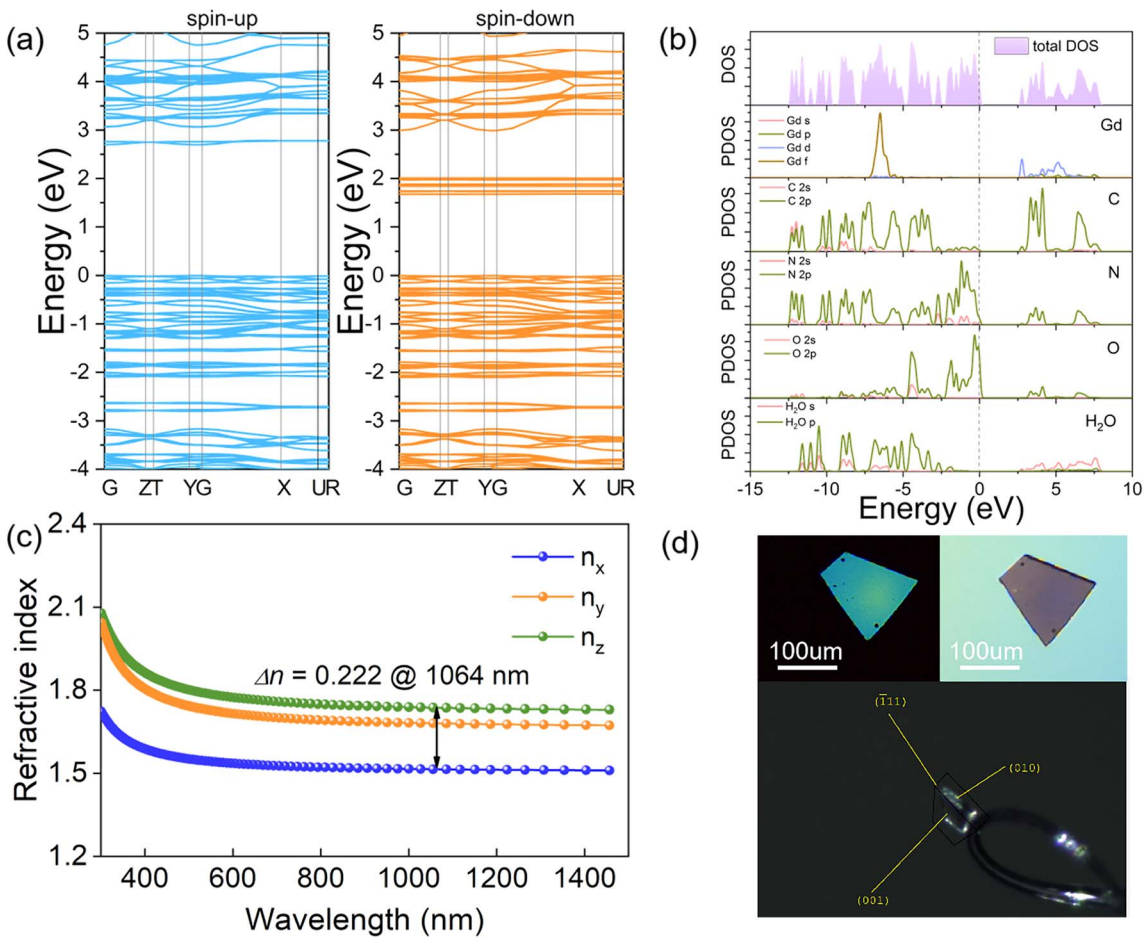

Fig. 3 (a) Calculated band structure of **II** and (b) DOS and partial DOS of **II**. (c) The calculated birefringence of **II**. (d) The original and the extinction state of the crystal plane (001) of **II**.

phonon coupling effect between rare-earth ions and their surrounding lattices.

Magnetic properties

The temperature-dependent magnetic susceptibility (χ) and its inverse ($1/\chi$) for compound **II** are presented in Fig. 2e. The magnetic susceptibility data of compound **II** is fitted to a modified Curie–Weiss (C–W) law: $\chi = C/(T - \Theta)$, where C is the Curie constant and Θ is the Weiss temperature. As shown, compound **II** obeys the C–W law and is paramagnetic. The effective magnetic moment μ_{eff} is 6.97 μ_B for the high-temperature region (100–280 K), which matches the theoretical value for Gd^{3+}. For the low-temperature range (2–10 K), the derived value of Θ for compound **II** is −0.54 K, which suggests weak magnetic exchange interactions among the adjacent Gd^{3+} cations.[37–39] The magnetization saturates around 5 T when the temperature is 2 K in compound **II** (Fig. 2f). Combining the strong optical nonlinearity, ultraviolet fluorescence, and paramagnetic behaviour, the $Gd(H_{1.5}C_6N_7O_3)_2\cdot 10H_2O$ (**II**) crystal is expected to be a promising multi-functional material in optoelectronic applications.

Theoretical calculations

To explore the origin of the second-order nonlinear optics, the electronic structure of compound **II** was calculated. As shown in Fig. 3a, it is a direct-gap semiconductor with a spin-up gap of 2.71 eV and a spin-down gap of 1.67 eV. Furthermore, the spin-up density of states (DOS) and partial density of states (PDOS) of **II** are analyzed. Fig. 3b depicts that the contribution from crystalline water molecules is negligible, and the valence band maximum and the conduction band minimum were primarily occupied by N 2p orbitals together with O 2p and C 2p orbitals, indicating the contribution of conjugated π-bonds. Interestingly, not only unoccupied C p, N p, and O p orbitals but also Gd d and f orbitals contribute to the bottom of the conduction band, corresponding to the clear participation of the rare earth Gd in the construction of energy band structures. Therefore, it should be the synergistic effect of the rare-earth ion and the large π-conjugated group that determines the optical response of $Gd(H_{1.5}C_6N_7O_3)_2\cdot 10H_2O$. For the Y and Lu-analogues, their band structure and PDOS were plotted in Fig. S7 and S8.†

Furthermore, the calculated optical anisotropy of compound **II** exhibits a large variation from the visible to near-IR region with $n_z > n_y > n_x$. As shown in Fig. 3c, the calculated birefringence $n_z - n_x$ is 0.22 at 1.06 μm, which is comparable to the commercialized birefringent crystal α-BBO (Δn ~0.12) and calcite (Δn ~0.17).[40,41] The calculated refractive index of **I** and **III** was given in Fig. S9† and the Δn_{cal} is around 0.2. In addition, the in-plane birefringence of single crystals **I**, **II**, and **III** was estimated experimentally by using orthogonal polarization

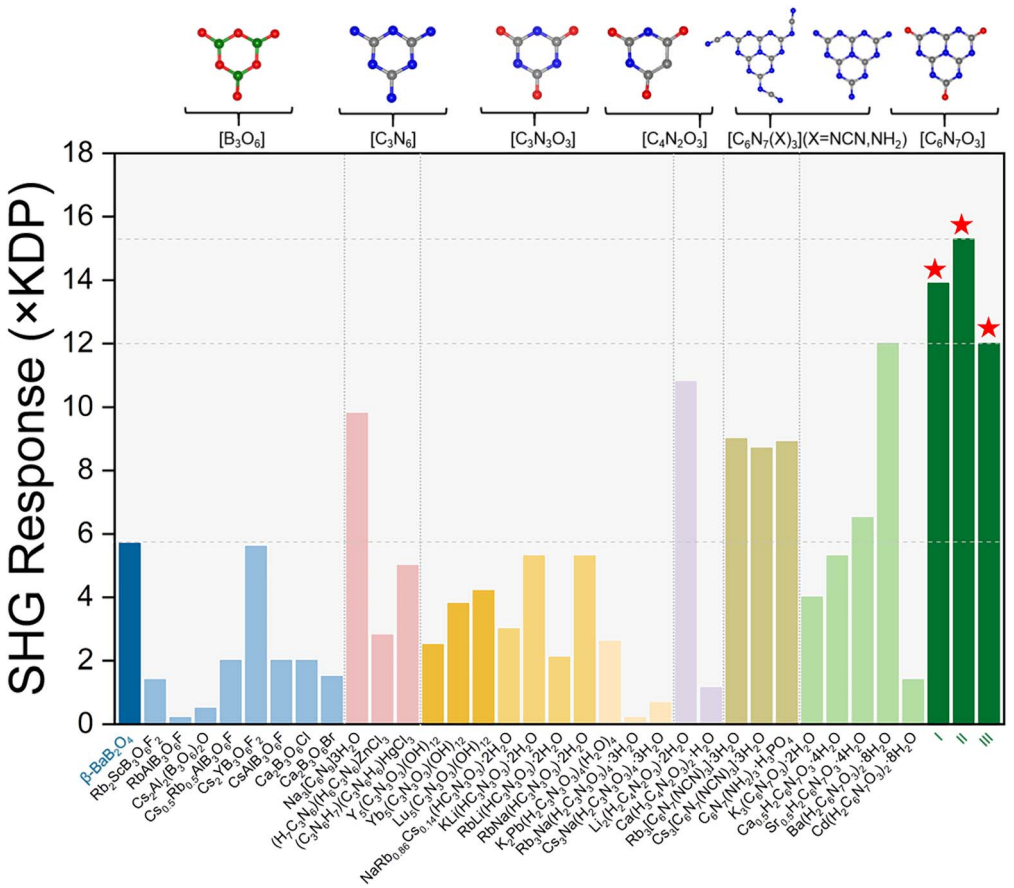

Fig. 4 SHG response of the compounds containing six-member ring B_3O_6-type π-conjugated groups and large C_6N_7-type π-conjugated groups.

microscopy with a halogen lamp.[42] The measured values of **I**, **II**, and **III** are all around 0.20 (Fig. 3d and S10†), which also agree well with the calculated values. This suitable optical anisotropy could be due to the large π-conjugated interaction of the cyamelurate $(C_6N_7O_3)^{3-}$ groups.

Moreover, Fig. 4 displays the reported SHG intensities of the compounds containing a single kind of FBUs of large π-conjugated $(B_3O_6)^{3-}$,[43–47] $(C_3N_6)^{6-}$,[48–50] $(C_3N_3O_3)^{3-}$,[51–55] and $(C_4N_2O_3)^{2-}$ groups,[56,57] and large π-conjugated groups of $[C_6N_7(NCN)_3]^{3-}$,[58] $[C_6N_7(NH)_2]$,[59] and $(C_6N_7O_3)^{3-}$.[26–31] The commercialized NLO crystal BBO was plotted as a benchmark crystal with a strong SHG response of 5.6 × KDP. As classical (B_3O_6)-type units, the contribution of the FBUs could favor the SHG response reaching up to 5.6 × KDP for recently discovered borate of $CsYB_3O_6F$, 5.3 × KDP for (iso)-cyanurates of $KLi(HC_3N_3O_3)\cdot 2H_2O$/$RbNa(HC_3N_3O_3)\cdot 2H_2O$, and 10.8 × KDP for the barbiturate of $Li_2(H_2C_4N_2O_3)\cdot 2H_2O$. In contrast, the compounds with large π-conjugated FBUs, such as $[C_6N_7(NCN)_3]^{3-}$, $[C_6N_7(NH)_2]$ and $(C_6N_7O_3)^{3-}$, generally exhibit larger SHG effects with a greater possibility than metal borates/cyanurates (>4 × KDP).

Among the large π-conjugated FBUs constructed compounds, only $Cd(H_2C_6N_7O_3)_2\cdot 4H_2O$ displays small SHG signals < 2 × KDP, while $A_3[C_6N_7(NCN)_3]\cdot 8H_2O$ (A = Rb, Cs)/$Ba(H_2C_6N_7O_3)_2\cdot 8H_2O$ can even reach the SHG intensities around 10 × KDP. Remarkably, benefiting from the synergistic effects of the large π–conjugated $(C_6N_7O_3)^{3-}$ group and rare earth metals, compounds **I**, **II**, and **III** exhibit extraordinary second-order harmonic generation (SHG) properties (13.9, 15.3, 12 × KDP, respectively) far beyond those reported previously for π-conjugated NLO compounds. To the best of our knowledge, this represents the strongest SHG effect among all π-conjugated NLO crystals, indicating the great contribution of $(H_xC_6N_7O_3)^{3-x}$ units for strengthening the nonlinear optical response.

Conclusions

Three new cyamelurate crystals of $RE(H_{1.5}C_6N_7O_3)_2\cdot 10H_2O$ (RE = Y, Gd, Lu) containing large π-conjugated orbitals were successfully synthesized. The three compounds displayed very strong SHG activity, sufficient birefringence, paramagnetic behaviour in the Gd-analogue, and broadband ultraviolet photoluminescence concurrently, suggesting that this series of compounds could be promising multi-functional optical materials. We believe this work provides a feasible approach for designing novel high-performance (iso)-cyamelurates and enriching new multi-functional integrated optoelectronic crystals, pointing to applications such as self-frequency doubling, magneto-optical switches, magnetoelectric coupling, and broadband fluorescent response.

Data availability

All data are available in the article and the ESI† or can be made available from the corresponding authors upon reasonable request. CCDC deposition numbers 2385148–2385150 (for compounds **I**, **II**, and **III**) contain the supplementary crystallographic data for this paper. By emailing data_request@ccdc.cam.ac.uk, or by contacting the Cambridge Crystallographic Data Centre, 12 Union Road, Cambridge CB2 1EZ, UK: fax: +44 1223 336033.

Author contributions

Jing Zhang: Investigation, writing – original draft; Yuxiao Liu: Investigation; Fangyan Wang: Investigation; Pifu Gong: Investigation; Zhaoyi Li: Investigation; Xinyuan Zhang: Investigation, writing-review & editing; Fei Liang: Theoretical calculations, writing-review & editing; Shu Guo: Investigation, formal analysis; Zhanggui Hu: Supervision; Yicheng Wu: Supervision.

Conflicts of interest

There are no conflicts to declare.

Acknowledgements

This work is supported by the National Natural Science Foundation of China (Grant No. 52272007, 52422201, 52372010, 22275201, and 22205091), National Key Research and Development Program of China (2021YFA0717800), and Natural Science Foundation of Shandong Province (ZR2023ZD53).

Notes and references

1 C. T. Chen, Y. C. Wu and R. K. Li, *Int. Rev. Phys. Chem.*, 1989, **8**, 65–91.
2 L. Wu, C. Lin, H. Tian, Y. Zhou, H. Fan, S. Yang, N. Ye and M. Luo, *Angew. Chem., Int. Ed.*, 2023, **63**, e202315647.
3 M. Mutailipu, J. Li and S. Pan, *Adv. Funct. Mater.*, 2024, 2419204.
4 M. Mutailipu, J. Han, Z. Li, F. Li, J. Li, F. Zhang, X. Long, Z. Yang and S. Pan, *Nat. Photonics*, 2023, **17**, 694–701.
5 Y. Chu, H. S. Wang, Q. Chen, X. Su, Z. Chen, Z. Yang, J. Li and S. Pan, *Adv. Funct. Mater.*, 2023, **34**, 2314933.
6 R. L. Tang, D. X. Yang, L. Ma, Y. L. Lv, W. Liu and S. P. Guo, *Adv. Opt. Mater.*, 2024, 2403044.
7 L. Qi, X. Jiang, K. Duanmu, C. Wu, Z. Lin, Z. Huang, M. G. Humphrey and C. Zhang, *J. Am. Chem. Soc.*, 2024, **146**, 9975–9983.
8 Y. Kang, C. Yang, J. Gou, Y. Zhu, Q. Zhu, W. Xu and Q. Wu, *Angew. Chem., Int. Ed.*, 2024, **63**, e202402086.
9 D. Dou, Q. Shi, H. Li, B. Zhang, D. Yang and Y. Wang, *Adv. Sci.*, 2024, **11**, 2401325.
10 J. Chen, C. L. Hu, X. H. Zhang, B. X. Li, B. P. Yang and J. G. Mao, *Angew. Chem., Int. Ed.*, 2020, **59**, 5381–5384.
11 X. Liu, L. Kang, P. Gong and Z. Lin, *Angew. Chem., Int. Ed.*, 2021, **60**, 13574–13578.
12 M. Mutailipu, F. Li, C. Jin, Z. Yang, K. R. Poeppelmeier and S. Pan, *Angew. Chem., Int. Ed.*, 2022, **61**, e202202096.
13 C. Wu, G. Wei, X. Jiang, Q. Xu, Z. Lin, Z. Huang, M. G. Humphrey and C. Zhang, *Angew. Chem., Int. Ed.*, 2022, **61**, e202208514.

14 K. Chen, C. Lin, J. Chen, G. Yang, H. Tian, M. Luo, T. Yan, Z. Hu, J. Wang, Y. Wu, N. Ye and G. Peng, *Angew. Chem., Int. Ed.*, 2023, **62**, e202217039.
15 P.-F. Li, C.-L. Hu, J.-G. Mao and F. Kong, *Mater. Horiz.*, 2024, **11**, 1704–1709.
16 Q. Zhang, R. An, X. Long, Z. Yang, S. Pan and Y. Yang, *Angew. Chem., Int. Ed.*, 2024, e202415066.
17 C. T. Chen, G. L. Wang, X. Y. Wang and Z. Y. Xu, *Appl. Phys. B*, 2009, **97**, 9–25.
18 C. T. Chen, B. C. Wu, A. D. Jiang and G. M. You, *Sci. China B*, 1985, **28**, 235–243.
19 C. T. Chen, Y. C. Wu, A. D. Jiang, B. C. Wu, G. M. You, R. K. Li and S. J. Lin, *J. Opt. Soc. A. B*, 1989, **6**, 616–621.
20 D. Lin, M. Luo, C. Lin, F. Xu and N. Ye, *J. Am. Chem. Soc.*, 2019, **141**, 3390–3394.
21 X. Meng, F. Liang, J. Tang, K. Kang, Q. Huang, W. Yin, Z. Lin and M. Xia, *Eur. J. Inorg. Chem.*, 2019, **23**, 2791–2795.
22 X. Meng, X. Zhang, Q. Liu, Z. Zhou, X. Jiang, Y. Wang, Z. Lin and M. Xia, *Angew. Chem., Int. Ed.*, 2022, **62**, e202214848.
23 F. Liang, L. Kang, X. Zhang, M.-H. Lee, Z. Lin and Y. Wu, *Cryst. Growth Des.*, 2017, **17**, 4015–4020.
24 Y. Chen, C. Hu, Z. Fang, Y. Li and J. Mao, *Inorg. Chem.*, 2022, **61**, 1778–1786.
25 D. Dou, Q. Shi, H. Li, B. Zhang, D. Yang and Y. Wang, *Adv. Sci.*, 2024, **11**, 2401325.
26 X. Zhang, X. Du, J. Wang, F. Wang, F. Liang, Z. Hu, Z. Lin and Y. Wu, *ACS Appl. Mater. Interfaces*, 2022, **14**, 53074–53080.
27 X. Du, F. Wang, F. Liang, Z. Hu, Y. Wu and X. Zhang, *Inorg. Chem. Front.*, 2023, **10**, 5979–5985.
28 Y. Li, W. Huang, Y. Zhou, X. Song, J. Zheng, H. Wang, Y. Song, M. Li, J. Luo and S. Zhao, *Angew. Chem., Int. Ed.*, 2023, **62**, e202215145.
29 Y. Li, X. Zhang, J. Zheng, Y. Zhou, W. Huang, Y. Song, H. Wang, X. Song, J. Luo and S. Zhao, *Angew. Chem., Int. Ed.*, 2023, **62**, e202304498.
30 N. E. Braml and W. Schnick, *Z. Anorg. Allg. Chem.*, 2012, **639**, 275–279.
31 A. S. Isbjakowa, V. V. Chernyshev, V. A. Tafeenko and L. A. Aslanov, *Struct. Chem.*, 2022, **33**, 607–615.
32 M. Essalhi, M. Mohan, G. Marineau-Plante, A. Schlachter, T. Maris, P. D. Harvey and A. Duong, *Dalton Trans.*, 2022, **51**, 15005–15016.
33 W. Wang, Z. Chen, X. Yang, P. Audebert, S. Sahoo, J. Chen, Y. Liu, S. Pamir Alpay, L. Xie and G. Wei, *Appl. Catal. A Gen.*, 2022, **641**, 118669.
34 S. K. Kurtz and T. T. Perry, *J. Appl. Phys.*, 1968, **39**, 3798–3813.
35 E. Horvath-Bordon, E. Kroke, I. Svoboda, H. Fueß, R. Riedel, S. Neeraj and A. K. Cheetham, *Dalton Trans.*, 2004, **22**, 3900–3908.
36 L. Zhang, F. Wang, X. Zhang, F. Liang, Z. Hu and Y. Wu, *Cryst. Growth Des.*, 2024, **24**, 627–631.
37 W. Yin, K. Feng, W. Wang, Y. Shi, W. Hao, J. Yao and Y. Wu, *Inorg. Chem.*, 2012, **51**, 6860–6867.
38 M. Ashtar, Y. Bai, L. Xu, Z. Wan, Z. Wei, Y. Liu, M. A. Marwat and Z. Tian, *Inorg. Chem.*, 2021, **60**, 3626–3634.
39 T. Wang, R. Guo, Q. Liu, Q. Wu, X. Meng, Z. Zhou, S. Guo and M. Xia, *Inorg. Chem.*, 2024, **63**, 13171–13175.
40 V. P. Solntsev, E. G. Tsvetkov, V. A. Gets, *et al.*, *J. Cryst. Growth*, 2002, **236**, 290–296.
41 G. Ghosh, *Opt. Commun.*, 1999, **163**, 95–102.
42 B. E. Sorensen, *Eur. J. Mineral.*, 2013, **25**, 5–10.
43 H. Liu, B. Zhang, L. Li and Y. Wang, *ACS Appl. Mater. Interfaces*, 2021, **13**, 30853–30860.
44 Z. Fang, X. Jiang, M. Duan, Z. Hou, C. Tang, M. Xia, L. Liu, Z. Lin, F. Fan, L. Bai and C. Chen, *Chem.–Eur. J.*, 2018, **24**, 7856–7860.
45 H. Wu, Z. Wei, Z. Hu, J. Wang, Y. Wu and H. Yu, *Angew. Chem., Int. Ed.*, 2024, **63**, e202406318.
46 H. Liu, Y. Wang, B. Zhang, Z. Yang and S. Pan, *Chem. Sci.*, 2020, **11**, 694–698.
47 H. Qiu, F. Li, Z. Li, Z. Yang, S. Pan and M. Mutailipu, *J. Am. Chem. Soc.*, 2023, **145**, 24401–24407.
48 Y. Li, Q. Wu, Z. Lin, Y. Liu, Y. Zhou, X. Chen, M. Li, M. Hong, J. Luo and S. Zhao, *Fund. Res.*, 2023, **3**, 974–978.
49 L. Liu, Z. Bai, L. Hu, D. Wei, Z. Lin and L. Zhang, *J. Mater. Chem. C*, 2021, **9**, 7452–7457.
50 Z. Bai, J. Lee, H. Kim, C. L. Hu and K. M. Ok, *Small*, 2023, **19**, 2301756.
51 J. Lu, Y.-K. Lian, L. Xiong, Q.-R. Wu, M. Zhao, K.-X. Shi, L. Chen and L.-M. Wu, *J. Am. Chem. Soc.*, 2019, **141**, 16151–16159.
52 X. Meng, F. Liang, K. Kang, J. Tang, T. Zeng, Z. Lin and M. Xia, *Inorg. Chem.*, 2019, **58**, 11289–11293.
53 Y. Song, D. Lin, M. Luo, C. Lin, Q. Chen and N. Ye, *Inorg. Chem. Front.*, 2020, **7**, 150–156.
54 Y. Chen, C. Hu, Z. Fang and J. Mao, *Inorg. Chem. Front.*, 2021, **8**, 3547–3555.
55 M. Aibibula, L. Wang and S. Huang, *ACS Omega*, 2019, **4**, 22197–22202.
56 D. Lin, M. Luo, C. Lin, L. Cao and N. Ye, *Cryst. Growth Des.*, 2020, **20**, 4904–4908.
57 Y. Xu, C. Lin, D. Lin, M. Luo, D. Zhao, L. Cao and N. Ye, *Inorg. Chem.*, 2020, **59**, 15962–15968.
58 D. Dou, B. Zhang, D. Yang and Y. Wang, *Chem. Sci.*, 2024, **15**, 19496–19503.
59 R. Wei, H. Huang, D. Yang, Y. Wang and B. Zhang, *Adv. Opt. Mater.*, 2024, **12**, 2401814.